2019-06-16

Smoothed Particle Hydrodynamics (SPH) Modelling of Tsunami Waves Generated by a Fault Rupture

Wana, R

The Proceedings of the 29th (2019) International Ocean and Polar Engineering Conference

Smoothed Particle Hydrodynamics (SPH) Modelling of Tsunami Waves Generated by a Fault Rupture

Ruaa Wana [a], Natalia Perez del Postigo Prieto [b],
Jason Hughes [a], David Graham [a], Alison Raby [b], and Colin Whittaker [c]
[a] School of Computing, Electronics and Mathematics, University of Plymouth, UK
[b] School of Engineering, University of Plymouth, UK
[c]Civil and Environmental Engineering, University of Auckland, New Zealand

ABSTRACT

In this paper we use a single phase weakly compressible SPH model to simulate the flow that occurs in experimental models of tsunamis generated by an earthquake fault rupture. The experiments have been carried out at University of Plymouth's COAST laboratory. Fortran code has been written to implement the SPH method. In order to obtain a good SPH particle distribution in the vicinity of the moving plate, and accurate predictions, careful consideration of the SPH boundary conditions is required. SPH simulations have been carried out using the ghost boundary particle method to implement boundary conditions. The SPH model gives generally good predictions of the free surface elevation.

KEY WORDS: Smoothed Particle Hydrodynamics (SPH), Tsunami Waves, Free Surface Flow.

INTRODUCTION

The smoothed particle hydrodynamic (SPH) method was developed by Gingold & Monaghan (1982) and has since been used in many areas of solid and fluid dynamics. It was first applied to solve astrophysical problems (Monaghan & Lattanzio 1985). In Weakly Compressible Smoothed Particle Hydrodynamics (WCSPH) (Monaghan, 1994; Morris et al. 1997), a stiff equation of state is used to compute the pressure directly from the particle density, rather than solving a linear system of equations (as is required in incompressible SPH models), which is computationally expensive. Any fluctuations in density would typically be around one per cent, due to the numerical speed of sound used, which is often taken as ten times the maximum fluid velocity.

In this paper, we describe the SPH model used, and in particular, the boundary conditions needed to obtain an accurate and stable solution. The experiments are described, and then we consider the effects of the length of the SPH model wave tank on the surface elevation predictions obtained. It would be computationally expensive to simulate the full length of the experimental wave tank. Therefore, we use an SPH model wave tank that is sufficiently long so that the predictions of surface elevation, at the wave gauge locations considered, are not influenced by the end wall of the tank. The SPH predicted surface elevations are then compared with the experimental measurements, which are generally in good agreement. There is also a discussion of possible reasons for any differences between the SPH simulations and the experiments. The surface profiles have also been used to calculate wave speeds, and there is reasonably good agreement between the SPH simulations, experiments and theory.

GOVERNING EQUATIONS

The Navier-Stokes equations together with the continuity equation for a viscous fluid are:

$$\begin{aligned} \frac{D\mathbf{u}}{Dt} &= -\frac{1}{\rho}\nabla P + \nu\nabla^2\mathbf{u} + \mathbf{f}, \\ -\frac{1}{\rho}\frac{D\rho}{Dt} &+ \nabla\cdot\mathbf{u} = 0, \end{aligned} \tag{1}$$

where $\mathbf{u}$ represents the velocity, t is the time, ρ is the density, P is the pressure, ν is the kinematic viscosity, $\mathbf{f}$ is the body force on the fluid, ∇ is the gradient operator, ∇^2 is the Laplacian operator, $\nabla\cdot$ is the divergence operator and $\frac{D}{Dt}$ is the convective derivative. The bold type represents vector quantities.

In this work, we use a standard SPH approximation as defined in Monaghan (1994).

Kernel function

In this work, for the best accuracy in 2D simulations, we use the quintic kernel function (Wendland function), which takes the form (Wendland,1995):

$$W_{ab} = \frac{7}{4\,\pi h^2}\left(1-\frac{q}{2}\right)^4 (2q+1) \quad \text{for} \quad 0 \le q \le 2, \tag{2}$$

where $q = r_{ab}/h$, r_{ab} is the distance between particles a and b, and h is the smoothing length of the kernel function.

Previous simulations, such as a dam break flow, have shown that we do not need to use a tensile instability correction if we use the Wendland kernel function. This makes the simulations computationally quicker.

Conservation of mass

As the simulations involve a free surface, it is necessary to calculate the particle density by evolving the density using equation (3) which defines the rate of change of density at a particle as

$$\frac{d\rho_a}{dt} = \sum_b m_b\,(\mathbf{u}_a - \mathbf{u}_b)\cdot\nabla_a W_{ab}, \tag{3}$$

where m is the mass of the SPH particles.

If the density was calculated using an SPH summation, then there would be an inaccurate lower density at the free surface, due to a deficit of SPH particles within the kernel region of influence of particles at or near the free surface. Equation (3) is used to evolve the density, by using an appropriate time stepping method to calculate the density of a particle at a given time. Also, we use density reinitialization which is described later in this paper.

Conservation of momentum

To formulate the conservation of momentum in SPH, we need to calculate the pressure and the viscous forces. The acceleration of a particle is defined by:

$$\frac{d\mathbf{u}_a}{dt} = f_a - \sum_b m_b\,(P_a + P_b)\,\nabla_a W_{ab} + \pi_{ab}, \tag{4}$$

where π_{ab} is a viscosity term, and in this work we use the laminar viscosity model (Morris et al. 1997) defined as:

$$\pi_{ab} = \sum_b m_b \frac{(\mu_a+\mu_b)\,\mathbf{r}_{ab}\cdot\nabla_a W_{ab}}{\rho_a\rho_b}\mathbf{u}_{ab}, \tag{5}$$

where μ is the dynamic viscosity.

Pressure formulation

In the SPH simulations of water, we use a stiff equation of state (Batchelor, 1967). Monaghan (1994) applied this equation of state for water to model free surface flows:

$$P = \frac{c_s^2\rho_0}{\gamma}\left(\left(\frac{\rho}{\rho_0}\right)^\gamma - 1\right), \tag{6}$$

where c_s is the speed of sound and is chosen as ten times the maximum fluid velocity, ρ_0 is the initial density and γ is a constant and usually chosen to equal 7 in water simulations, so that large pressure variations can be obtained with small variations in density.

Also, we initialise the particle density so that the initial pressure solution is hydrostatic. The initial density is used to produce an initial hydrostatic pressure from the stiff equation of state, by setting the initial density from

$$\rho(y) = \rho_0\left(1+\frac{\rho_0 g(H-y)}{c_s^2\rho_0}\right)^{\frac{1}{\gamma}}, \tag{7}$$

where H is the initial water depth, y is the vertical particle position measured from the base of the wave tank and the other parameters are as defined for equation (6).

In the present work, it was found that modifying the pressure boundary condition, by adding a hydrostatic pressure gradient (ρg) to the dummy particles below the moving plate and the floor of the wave tank, enhances the results obtained. In SPH simulations of a still water tank, adding a hydrostatic pressure gradient (ρg) to the dummy particles at the base of the water tank was required in order to maintain a hydrostatic pressure solution over time.

Density reinitialization

In SPH simulations, unphysical pressure oscillations can occur, which are a result of fluctuations in the density. In this work, we use a Shepard filter which is a quick and simple correction to the density field, and the following procedure is applied, usually every ten time steps, in the simulations (Crespo, 2008):

$$\rho_a^{new} = \sum_b \rho_b \tilde{W}_{ab}\frac{m_b}{\rho_b} = \sum_b m_b \tilde{W}_{ab}, \tag{8}$$

where the kernel has been corrected using the zeroth-order correction:

$$\tilde{W}_{ab} = \frac{W_{ab}}{\sum_b W_{ab}\frac{m_b}{\rho_b}}. \tag{9}$$

In this work, we use a Shepard filter rather than the Moving Least Squares approach (Colagrossi & Landrini, 2003) because it is computationally quicker.

Boundary conditions

In SPH, quantities calculated for particles near the boundary of the flow region, will be affected if there is a deficit of particles within the interpolation domain. To avoid problems at the boundaries, and to actually define the location of the boundaries, dummy particles, outside of the flow region, are introduced.

There are various methods to impose boundary conditions in SPH. In this work, we have carried out simulations using both fixed dummy particles and ghost dummy particles and found that we obtained a more stable and accurate pressure solution if we use ghost dummy particles particles.

The fixed dummy particles are defined at regularly spaced positions behind a line of fixed wall particles, and their position does not change throughout the simulation. With the Wendland kernel function, we need two lines of fixed dummy particles.

The ghost particles are defined outside the fluid domain and are created when the fluid particles are close to the wall boundary, within a distance shorter than the kernel domain from any boundary wall. The purpose of the ghost particles is to exert a force on the fluid particles which prevent them moving outside of the flow boundaries. The pressure and density is the same as that of the corresponding fluid particles. In this work, a slip boundary condition is used on the solid walls of the flow geometry. Figure (1) shows a typical configuration of fluid and ghost particles at a wall boundary and also illustrates particle velocity components when a slip boundary is used. Figure (2) shows how ghost dummy particles are created to define the corner of the moving plate. In this region there will be ghost dummy particles created by reflecting fluid particles from 3 different fluid regions, 3, 4 and 5, with the corresponding ghost dummy particles denoted as type 3′, 4′ and 5′ respectively. Fluid particles in

a given region are then only influenced by the corresponding ghost dummy particles for that region. For example, fluid particles in region 3 would be influenced by ghost dummy particles of type 3′, but would not be influenced by ghost dummy particles of types 4′ and 5′. Figure 2 also shows the ghost dummy particles in the flow region at the edge of the moving plate, with a different colour used to represent each type of ghost dummy particle.

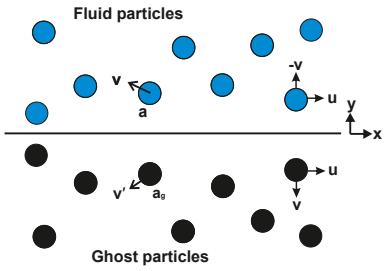

Fig. 1 Ghost particles.

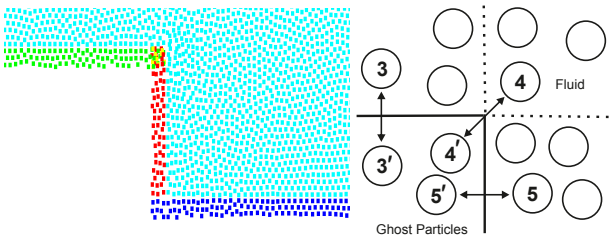

Fig. 2 Ghost particles creation at the corner of the moving plate.

Time stepping

In this work, we used an Euler time stepping scheme. First we update the velocity and density, then we calculate the XSPH velocity to use it in updating the particle position, as follows:

$$\mathbf{u}_a^{n+1} = \mathbf{u}_a^n + (\Delta t)\,\mathbf{F}_a^n,$$
$$\rho_a^{n+1} = \rho_a^n + (\Delta t)\,D_a^n,$$
$$\mathbf{u}_{XSPH} = \mathbf{u}_a + \epsilon \sum_b \frac{m_b}{\overline{\rho}_{ab}} \mathbf{u}_{ab} W_{ab}, \tag{10}$$
$$\mathbf{r}_a^{n+1} = \mathbf{r}_a^n + (\Delta t)\,\mathbf{u}_a^n + 0.5\,(\Delta t)^2\,\mathbf{F}_a^n,$$

where $\mathbf{F}_a^n = d\mathbf{u}_a/dt$, $D_a^n = d\rho_a/dt$, $\epsilon = 0.5$ and $\overline{\rho}_{ab} = \frac{1}{2}(\rho_a + \rho_b)$.

The use of Euler time stepping is computationally quicker than higher order time stepping schemes. In previous SPH simulations (lid driven cavity flow, still water tank and dam break flow) we have used a Verlet time stepping scheme, but found that there is very little difference between the solutions obtained using Euler or Verlet time stepping. Using the XSPH velocity correction ensures that the particles are more evenly distributed and that they are moved with a velocity closer to the average velocity in a given particles neighbourhood (Dalrymple and Rogers, 2006).

SIMULATION OF 2D TSUNAMI WAVE GENERATED BY FAULT RUPTURE

In this paper we use the SPH model described to simulate the flow that occurs in experimental models of tsunamis generated by an earthquake fault rupture. The experiments have been carried out at University of Plymouth's COAST laboratory, as part of a PhD project. Figure (3) shows a schematic representation of the wave tank. The SPH model consists of a truncated horizontal water tank, with a water depth of 0.3 m. We have carried out simulations for various length SPH model wave tanks in order to establish the effect of the end wall boundary conditions on the SPH simulations. The tsunami wave is generated by the rapid uplift of a plate on the bed of the tank, where it moves up very rapidly and the vertical displacement time history is shown in figure (4). The plate displacement profile is applied to the plate boundary in the SPH model. The uplifted plate is 0.6 m long x 0.6 m wide (the full width of the flume). The SPH simulations used approximately 250,000 particles, with a particle spacing of 0.003 m. The tank contains eight wave gauges (WG), and the distance between each wave gauge is 0.1 m, with the first located in line with the end of the moving plate. A slip boundary condition is used at the end wall in the SPH simulations.

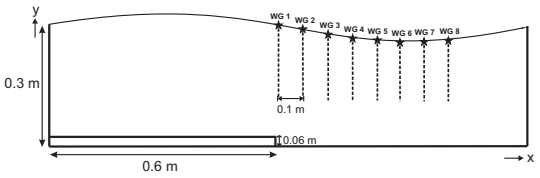

Fig. 3 Schematic representation of wave tank.

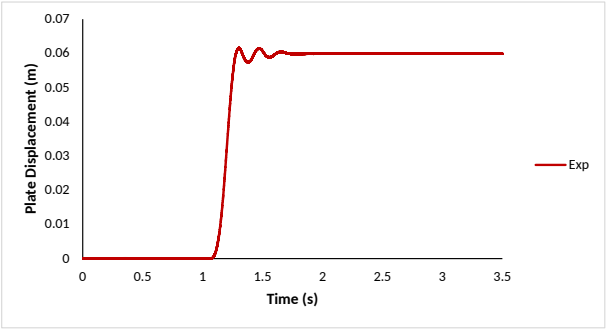

Fig. 4 Experiment plate displacement.

The experimental wave tank has a sloped ramp, of height 0.06 m and length 0.224 m, on the base of the wave tank, immediately to the right of the plate. This is so that the experimental tank can also be adapted for other experimental set ups, with a slope on top of the moving plate which aligns with the sloped ramp fixed to the base, when the plate has moved upwards. A landslide can also then be created down the continual slope. We have carried out SPH simulations which include the sloped ramp in the model, and, in terms of the free surface position, very similar results were obtained both with and without the sloped ramp in the SPH model. However, the SPH simulations that include the sloped ramp had an unstable pressure solution, which we believe was caused by the SPH particles close to the sloped ramp moving into an irregular configuration, as the simulation progressed in time. In future

work, we will consider using 'fixed' ghost dummy particles to define the sloped ramp, which should ensure a more regular particle configuration close to the sloped ramp and hence a more stable pressure solution.

SPH simulations have been carried out for model wave tanks of three different lengths (3 m, 5.5 m and 7.5 m), in order to establish if there is any effect of the SPH tank end wall boundary condition, on the predicted surface height over the time range considered, which was until approximately 2.5 seconds after the plate started moving. Figures (5) and (6) show the SPH predicted surface height at wave gauges 1 and 8 respectively, for the three different lengths of SPH model wave tank. It can be seen that very similar results are obtained at wave gauge 1 for each of the three different lengths and that for wave gauge 8, there is little difference in the surface height predictions obtained from the 5.5 m and 7 m length SPH wave tank simulations. Hence, we conclude that for the time range considered, the SPH surface height predictions at the wave gauge locations are not influenced by the SPH end wall boundary condition, if the length of the SPH wave tank is at least 5.5 m. It is noted that, with the wave speeds obtained in the experiments and the SPH simulations, the wave does not reach the end of the 5.5 m and 7.5 m length wave tanks, within the time range shown in these figures.

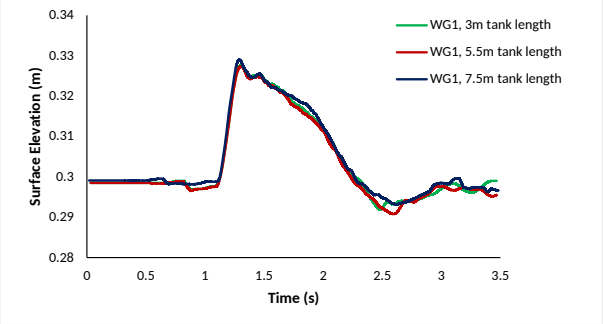

Fig. 5 Effect of tank length on WG1 surface elevation using SPH method.

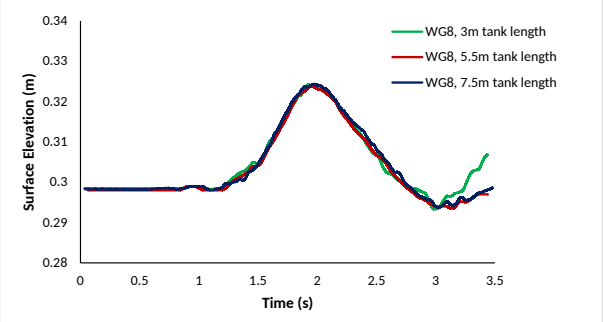

Fig. 6 Effect of tank length on WG8 surface elevation using SPH method.

An SPH interpolation of the density is calculated along vertical lines of fictitious points (each at a distance of $dx/10$ apart) at each wave gauge location and the free surface is defined where the SPH interpolated density is below a certain value (850 kg/m^3). Using a higher resolution of SPH particles decreases the 'noise' in the prediction of the free surface location, as shown in figure (7), where the SPH predicted surface height at wave gauge 1 is presented for initial particle spacings of $dx = 0.006$ and $dx = 0.003$.

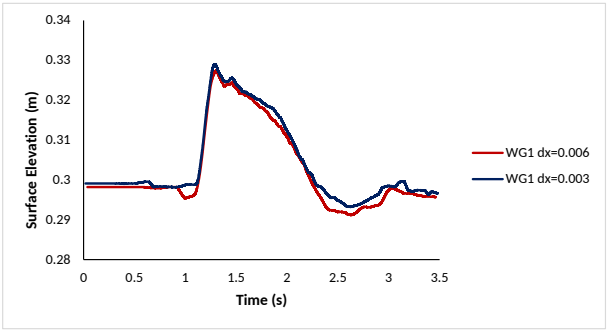

Fig. 7 Comparison of WG1 surface elevation using SPH method with two different particle resolution.

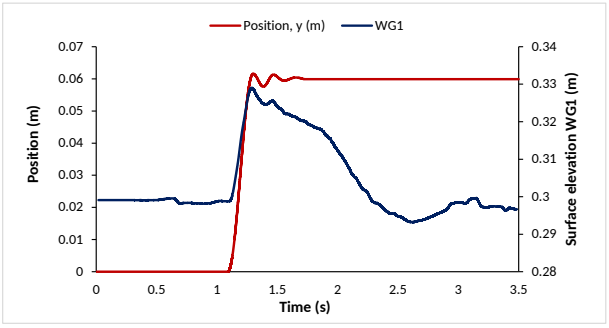

Fig. 8 SPH plate displacement and elevation at WG1.

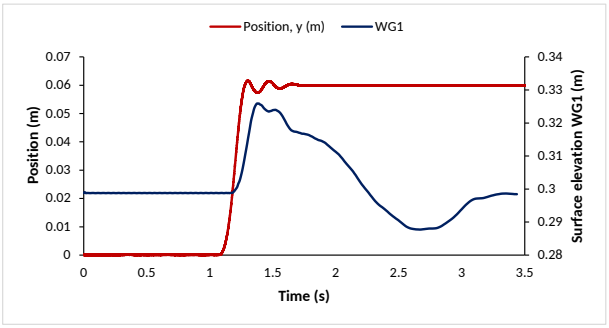

Fig. 9 Experiment plate displacement and elevation at WG1.

Figure (8) shows the SPH predicted surface height at the first wave gauge together with the plate displacement applied in the SPH simulations. It shows that the free surface at wave gauge 1 starts moving almost instantly after the plate starts moving. Figure (9) shows the same comparison for the experiments. From figures (8) and (9) we conclude that both the SPH simulation and experimental trends in free surface height at wave gauge 1 are similar. However, in the SPH simulations, the surface height rises more quickly after the plate starts moving, than

in the experiments. We believe that the difference is due to some water being able to move around below the plate, as it lifts upwards in the experiments, whereas in the SPH simulations all of the water is always above the plate. In the experiments, any movement of water from above to below the plate is through small gaps at the plate edges. If this were to be included in the SPH model, then it would not be possible to have a sufficient resolution of particles in the gaps without making the simulations too computationally expensive.

Figures (10) and (11) respectively show the SPH predictions and the experimental measurements of surface height at the eight wave gauges. In the SPH simulations and the experiments the plate starts moving at $t = 1.09$ s, so still water is simulated from $t = 0$ s to $t = 1.09$ s in the SPH model, which enables the SPH particles to settle in to a natural configuration before the plate starts moving. Note that initially, at $t = 0$ s, the SPH particles are positioned on a regular grid, which is not a natural configuration for the SPH particles. In figures (10) and (11) we see that in general, the SPH simulations correctly model the increase in surface height and the movement of the wave along the wave tank. There is agreement between the time at which the surface height starts to increase, and the peak height, at each of the wave gauge locations.

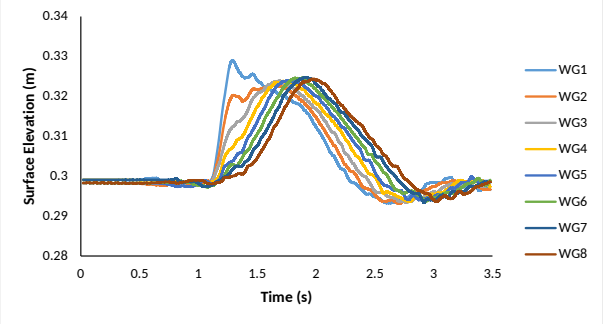

Fig. 10 SPH predictions of surface height at the eight different wave gauges.

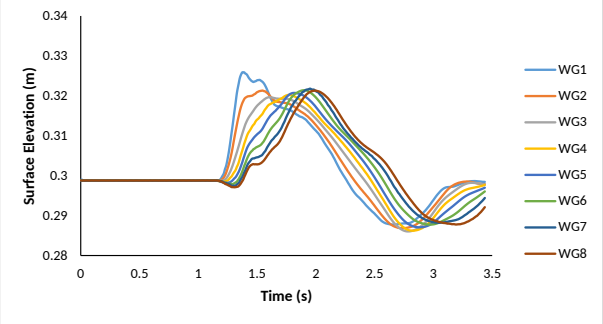

Fig. 11 Experimental measurements of surface height at the eight different wave gauges.

Figures (12) to (14) show a direct comparison between the SPH predictions and experimental measurements of surface height at selected wave gauges. In figures (10) to (14) it is seen that there are differences between the SPH and experimental surface elevations when the surface level falls, with the depth of trough under predicted in the SPH simulations. We believe that this is because, in the experiments, some water could move around below the plate as it moves upwards, whereas in the SPH model, all fluid remains above the plate at all times. For this reason, the largest differences between the SPH and experimental surface height profiles shown in figures (10) to (14) occur between $t = 2.5$ s and $t = 3.5$ s.

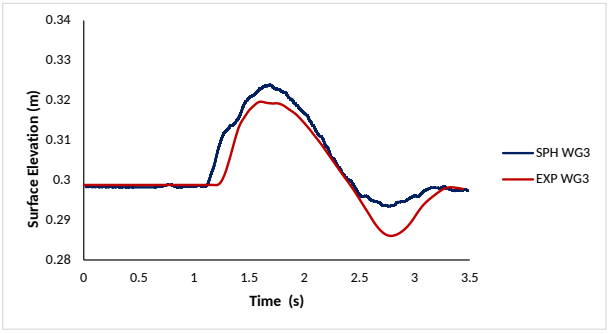

Fig. 12 Comparison between SPH predictions and experimental measurements of surface height at WG3.

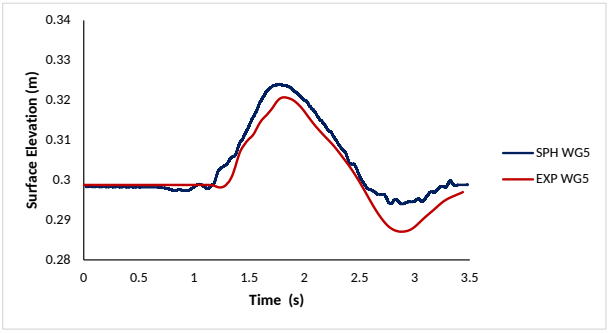

Fig. 13 Comparison between SPH predictions and experimental measurements of surface height at WG5.

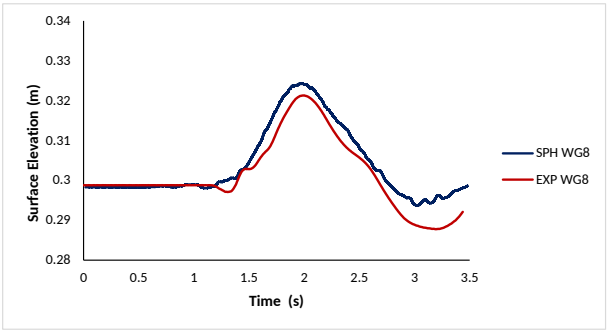

Fig. 14 Comparison between SPH predictions and experimental measurements of surface height at WG8.

The phase velocity, V_{ph}, or tsunami speed, of a shallow water gravity wave is defined in Truong (2012) as $V_{ph} = \sqrt{g(D + A)}$, where D is the

water depth and A is the wave amplitude. Using the wave amplitude at wave gauge 4 from both the SPH simulations and the experiments, V_{ph} is calculated as 1.78 m/s for the SPH simulations and 1.77 m/s for the experiments. We have calculated a tsunami wave speed using the peaks in the surface height profiles shown in figures (10) and (11). That is, we have used the time between the surface height peaks between two wave gauges (4 and 8), to calculate the speed at which the wave travels. These calculations give a SPH tsunami wave speed of 1.74 m/s and an experimental wave speed of 1.67 m/s. We have also calculated wave speeds by using the time difference in the zero crossing height between wave gauges 4 and 8. This gives a SPH tsunami wave speed of 1.74 m/s and an experimental wave speed of 1.74 m/s. These calculations show that there is reasonably good agreement between the wave speed obtained in the SPH simulations with that obtained in the experiments, and also with that predicted by the theory in Truong (2012).

Figure (15) shows the SPH pressure solution near the plate over the times at which it is moving upwards. Note that the plate moves upwards from $t = 1.09$ s to $t = 1.29$ s. In figure (15) it is seen that the initial hydrostatic pressure that was set at $t = 0$ s is maintained at $t = 1$ s and that there is an increase in pressure above the plate when it starts moving upwards at $t = 1.09$ s. Figure (16) shows the SPH predicted vertical velocity when the plate is half way up, at $t = 1.19$ s, and it is seen that in the section of water above the plate, it is all moving upwards at a very similar velocity. Figure (17) shows the SPH pressure solution, near the plate end of the SPH model tank, at various times after the plate has moved upwards, where it is seen that, as expected, the pressure settles to a hydrostatic solution. This figure also shows the shape of the wave and how it travels along the wave tank as time progresses.

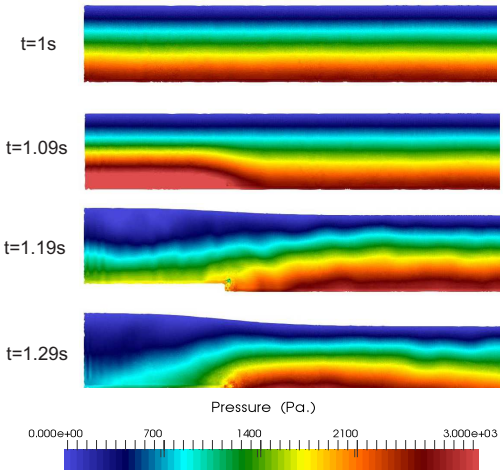

Fig. 15 SPH pressure solution near the plate over the times at which it is moving upwards.

CONCLUSIONS

In this paper, we used the SPH method to simulate the flow that occurs in experimental models of tsunamis generated by a fault rupture. The results show that the SPH model gives generally good predictions of the free surface position. At each wave gauge location, there is good agreement between the SPH predictions and experimental measurements of the peak surface height and also the time it takes for the free surface

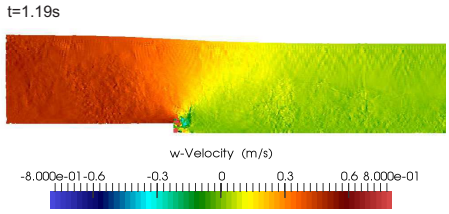

Fig. 16 SPH vertical velocity solution when the plate is half way up, at $t = 1.19$ s.

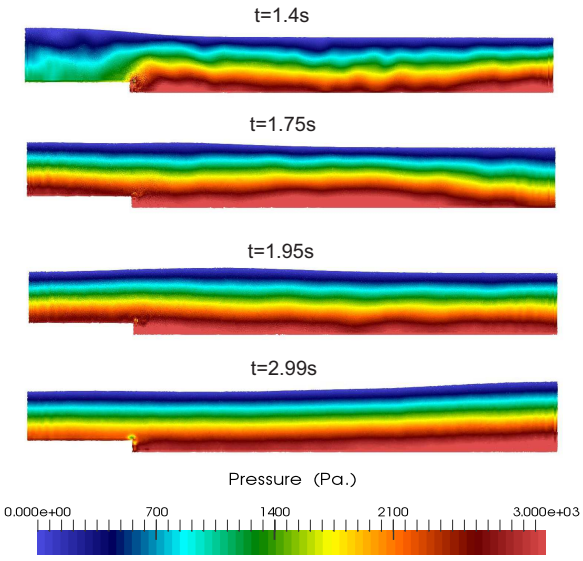

Fig. 17 SPH pressure solution at various times after the plate has moved upwards.

height to increase and then return to the zero crossing height. There is also agreement between the calculated wave speeds from the SPH simulations and the experiments. However, relative to when the plate starts moving upwards, the surface height rises more quickly in the SPH simulations than in the experiments and the trough depths are under predicted by the SPH model. We believe that these differences are due to some water being able to move around and below the moving plate in the experiments, whereas in the SPH model all of the water is always above the plate. The SPH simulations also show that, as expected, using a higher particle resolution decreases the noise in the predicted free surface location. In future work, we will consider SPH simulations of the more complex experiments, including a sloped ramp on top of the moving plate and a landslide.

REFERENCES

Batchelor, G. K. (1967), "*An introduction to fluid dynamics*", Cambridge University Press.

Crespo, A. J. C. (2008), "Application of the smoothed particle hydrodynamics model SPHysics to free surface hydrodynamics", *Universidade de Vigo*.

Colagrossi, A. & Landrini, M. (2003), "Numerical simulation of interfacial flows by smoothed particle hydrodynamics", *Journal of computational physics* **191**(2), 448-475.

Dalrymple, R. A. & Rogers, B. D. (2006), "Numerical modeling of water waves with the SPH method", *Coastal engineering* **53**(2-3), 141-147.

Gingold, R. A. & Monaghan, J. J. (1982), "Kernel estimates as a basis for general particle methods in hydrodynamics", *Journal of Computational Physics* **46**(3), 429-453.

Goffin, L., Archambeau, P., Pirotton, M., Dewals, B., Duchene, L. & Mouzelard, T. (2013), "Development of a didactic SPH model", *Liege: University of Liege (ULg)*.

Liu, G. R. & Liu, M. B. (2003), "*Smoothed particle hydrodynamics: a meshfree particle method*", World Scientific.

Monaghan, J. (1994), "Simulating free surface flows with SPH", *Journal of Computational Physics* , **110**(2), 399-406.

Monaghan, J. J. & Lattanzio, J. C. (1985), "A refined particle method for astrophysical problems", *Astronomy & Astrophysics* **149**, 135-143.

Morris, J. P., Fox, P. J. & Zhu, Y. (1997), "Modeling low reynolds number incompressible flows using sph", *Journal of Computational Physics* , **136**(2), 214-226.

Truong, H. V. P. (2012), "Wave-propagation velocity, Tsunami speed, amplitudes, dynamic water-attenuation factors", *In Proc. 15th World Conference on Earthquake Engineering (15WCEE)* , 24-28.

Vitanza, E. (2014), "Application of SPH numerical procedures to hydraulic problems", *Universit degli Studi di Palermo*.

Wendland, H. (1995), "Piecewise polynomial, positive definite and compactly supported radial functions of minimal degree", *Advances in Computational Mathematics*, **4**(1), 389-396.